Journal of Power Sources 227 (2013) 118–122

Contents lists available at SciVerse ScienceDirect

Journal of Power Sources

journal homepage: www.elsevier.com/locate/jpowsour

Short communication

Easy synthesis of honeycomb hierarchical porous carbon and its capacitive performance

Yan Han, Xiaoting Dong, Cui Zhang, Shuangxi Liu*

Institute of New Catalytic Materials Science, Key Laboratory of Advanced Energy Materials Chemistry (MOE), College of Chemistry, Nankai University, Tianjin 300071, PR China

HIGHLIGHTS

- Easy preparation method based on solvent evaporation.
- Unique hierarchical porous structure with interconnected meso/macropore and abundant micropore.
- Excellent electrochemical performances as capacitor electrode material.

ARTICLE INFO

Article history:
Received 23 August 2012
Received in revised form
6 November 2012
Accepted 16 November 2012
Available online 23 November 2012

Keywords:
Honeycomb-like
Hierarchical porous structure
Solvent evaporation
Supercapacitor

ABSTRACT

Honeycomb hierarchical porous carbon (HHPC) with interconnected meso/macropore and abundant micropore has been synthesized by an easy solvent evaporation method. The obtained HHPC as an electrode material exhibits good capacitive performances with a long cyclic life, a high specific capacitance of 292 F g^{-1} at 1 A g^{-1} in KOH aqueous electrolyte, and a low capacitance loss of 20% when the current density increased by 10 times.

1. Introduction

Supercapacitors have attracted rapidly increasing research interests because of their high power density, fast recharge capability and long cycle life. Activated carbon is the most widely adopted electrode material. But the slow ion transportation in the small micropores limits their effective utilization [1–3]. Thus, three-dimensionally meso/macroporous carbons with hierarchical porous structures, which facilitate ion transport by providing a smaller resistance and shorter diffusion pathways, are proposed to become high performance supercapacitor electrode materials. In recent years, many hierarchical porous carbons with different morphologies and structures have been successfully synthesized and applied as supercapacitor electrode materials, which show high capacitive performance and excellent rate capability [4–11]. We have prepared dispersed carbon hollow-spheres with micropore shells and meso/macropore cores by hydrothermal method and have revealed that the as-prepared material possesses high capacitive nature as a result of the hierarchical porous structure [12].

Here, honeycomb hierarchical porous carbon (HHPC) has been synthesized by an easy solvent evaporation method using glucose as carbon source and colloidal silica as template. The obtained HHPC possesses a unique three-dimensionally hierarchical porous structure with interconnected meso/macropore and abundant micropore, which facilitates the transport of electrolyte ions and offers a good environment for charge accumulation so as to give rise to excellent performances as an electrode material for supercapacitors.

2. Experimental

2.1. Materials synthesis and characterization

The synthesis of the HHPC was based on a simple solvent evaporation method using colloidal silica as template. The preparation procedure is illustrated in Fig. 1. First, the colloidal silica was prepared by Stöber method and surface modified by 3-aminopropyltrimethoxysilane (APMS) as reported previously [13,14].

* Corresponding author. Tel./fax: +86 22 23509005.
E-mail address: sxliu@nankai.edu.cn (S. Liu).

0378-7753/$ – see front matter © 2012 Elsevier B.V. All rights reserved.
http://dx.doi.org/10.1016/j.jpowsour.2012.11.054

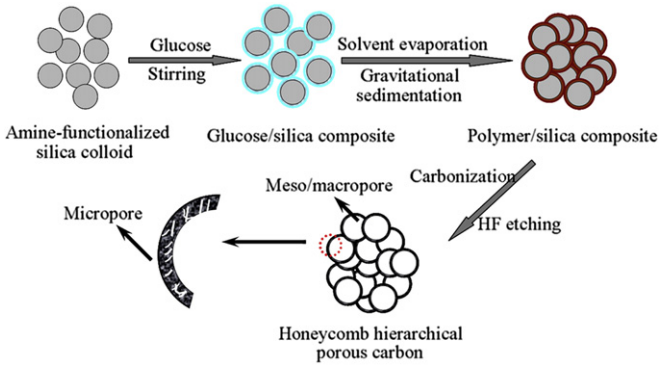

Fig. 1. Schematic illustration of the preparation process of the HHPC.

Then, glucose (0.2 g) was dissolved in the above silica colloid (20 ml) under stirring. Because the electrostatic interaction between ammonium groups on the surface of the colloidal silica spheres and hydroxyl groups of the glucose, the glucose can be absorbed and coated on the surface of the colloidal silica spheres. After solvent evaporation and gravitational sedimentation, the polymer/silica composite was obtained. Finally, the composite was carbonized at 800 °C for 2 h under N_2 flowing and etched by hydrofluoric acid (HF, 40 wt.%) to remove silica.

The morphology of the as-prepared HHPC was characterized by scanning electron microscopy (SEM, Hitachi S-4800), transmission electron microscopy (TEM, Philips Tecnai G^2 F20). Thermogravimetric analysis (TGA) was carried out on an NETZSCH TG 209 apparatus with a heating rate of 10 °C min^{-1} under air. Raman scattering was determined using a Renishaw inVia Raman spectrometer ($\lambda = 514.5$ nm). X-ray photoelectron spectroscopy (XPS) was performed on a Kratos Axis Ultra DLD with a Al Kα X-ray source. And nitrogen adsorption–desorption isotherms were measured with a Micromeritics ASAP 2020 analyzer at 77 K. The specific surface area (S_{BET}) was calculated from nitrogen adsorption isotherms using the Brunauer–Emmett–Teller (BET) method, whereas the total pore volume was determined by the single point method at $P/P_0 = 0.97$.

2.2. Electrochemical measurement

All electrochemical experiments were carried out using a three-electrode system at room temperature. For making a working electrode, as-prepared HHPC, acetylene black and polytetrafluoroethylene (PTFE) with a weight ratio of 90:5:5 were pressed between two pieces of 1 × 1 cm^2 nickel foam. The mass of porous carbon contained in each working electrode was between 3 and 5 mg. Before electrochemical tests, the electrodes were vacuum soaked with 6 M KOH aqueous solution. Electrochemical measurements were carried out with 6 M KOH aqueous solution as the electrolyte, Ni foil and Hg/HgO electrode as the counter and reference electrodes, respectively.

The cyclic voltammetry (CV) and electrochemical impedance spectroscopy (EIS) were performed on CHI 660D electrochemical analyzer. The galvanostatic charge–discharge tests were studied using LAND CT2001A instrument. The specific capacitance of the electrode was calculated according to the equation:

$$C = \frac{I\Delta t}{m\Delta V}$$

where I is the discharge current (A), Δt is the total discharge time (s), m is the mass of active material in the electrode (g) and ΔV is the potential range in the discharge process (V).

3. Results and discussion

The SEM and TEM micrographs of the HHPC are shown in Fig. 2. From the SEM images at different magnification (Fig. 2a and b), it can be observed that the sample is three-dimensionally honeycomb-like structure and the size of the interconnected pores is in the range of 30–50 nm, agreed well with the size of colloidal SiO_2 particles. Further details of the microstructure of HHPC can be seen that, shown in Fig. 2c, the pore arrangement of the sample synthesized is disordered. The thickness of the pore wall is very thin and only about 5 nm. From the higher-magnification image (Fig. 2d), it reveals a disordered microporous texture of the pore wall. And the microporous walls consist of localized graphitic structures, which lead to a large number of defects such as edges and pores (the inset in Fig. 2d).

Moreover, the graphitic structure of the HHPC is further studied by Raman spectroscopy (Fig. 3a). Two characteristic peaks around 1359 and 1593 cm^{-1} could be observed. The peak at 1593 cm^{-1}, known as the G band, corresponds to the stretching mode of C–C bonds of typical graphite. The band at 1359 cm^{-1}, known as the D band, is assigned to the defects and disorders in carbonaceous solid. The intensity ratio (I_D/I_G) of the two bands is about 0.83, verifying the low degree of graphitization of the as-obtained HHPC [15–17]. Thermogravimetric analysis (TGA) can provide information about the carbon content as well as the quality of the HHPC because the oxidation temperature reflects the material defect degree (Fig. 3b). The HHPC starts to oxidize at 450 °C, which is much lower than that of ideal graphite (600 °C). With the temperature increasing, the HHPC begins to decompose at 550 °C in air and is exhausted at 700 °C. The ash content of the HHPC after combustion at 900 °C is 0% w/w. These results indicate that the carbonization is carried out enough despite a high defect degree of the HHPC, and the obtained HHPC has high purity without SiO_2 residue.

X-ray photoelectron spectrum (XPS) was used to study the surface compositions of the HHPC. The survey scan spectrum shows the presence of carbon and oxygen (Fig. 4a). No signal related with silicon is observed, suggesting the silica is completely removed. This is well in accordance with the TGA result. The atomic ratio of (O 1s)/(C 1s) is 0.06, showing the moderate oxygen functional groups in the HHPC. Deconvolution of the O 1s peak (Fig. 4b) shows the presence of three oxygen-containing groups [18,19]: carbonyl groups (ca. 531.7 eV), ether groups (ca. 533.1 eV) and hydroxyl groups and chemisorbed water (ca. 534.2 eV). These functional groups could improve the wettability of the carbon surface and the specific capacitance of the carbon electrodes.

The N_2 adsorption–desorption isotherms of the HHPC (Fig. 5a) exhibit a combined characteristic of type I/IV, indicating the assembly of micro-, meso- and macro-pores. The total pore volume is 1.17 $cm^3\ g^{-1}$. The Brunauer–Emmett–Teller (BET) specific surface area is about 656 $m^2\ g^{-1}$ with the contribution of 271 $m^2\ g^{-1}$ from the micropore, revealing the presence of excessive micropores. The pore size distribution (PSD) curve (Fig. 5b) derived from the adsorption branch of the isotherm using the density functional theory (DFT) method clearly shows well-developed pore system with detectable sizes of 1.5 and 40 nm. The micropores with sizes of 0.4–2 nm and a maximum peak at 1.5 nm are generated from the carbonization process, which are efficient to accumulate charges [20]. While the mesopores and macro-pores with a maximum peak at 40 nm are contributed from the removal of the SiO_2 template embedded in the carbon matrix and dispersed on the surface, respectively. Those results agree well with above data derived from the SEM/TEM measurements (Fig. 2a–d). On the basis of these results, it can be concluded that the HHPC has a three-dimensionally hierarchical pore structure with interconnected

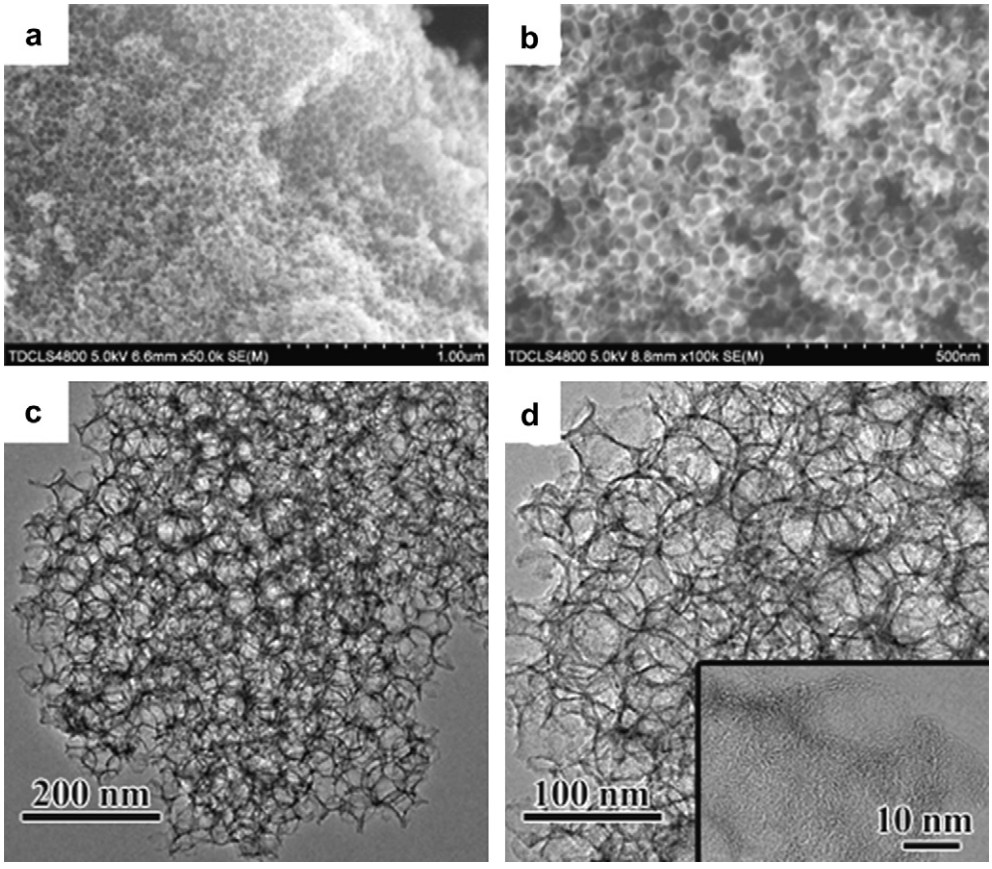

Fig. 2. Typical SEM (a, b) and TEM (c, d) micrographs of the HHPC at different magnification. The inset in (d) is the high-resolution TEM of the localized graphitic walls.

meso/macropore and abundant micropore, which may be helpful for ion diffusion and storage.

The electrochemical performances of the as-prepared HHPC as a capacitor electrode material were evaluated by CV, EIS and galvanostatic charge–discharge measurements in 6 M KOH aqueous solution.

The CV curves (Fig. 6a) measured at different scan rates all display near rectangular shapes with slightly distorted, which are characteristic of electrochemical capacitor [18,21–23]. With the increase of the scan rate, the current density increases gradually but the shape of the curves maintains with only slight distortion, indicating a small equivalent series resistance (ESR) and excellent capacitive nature of the HHPC [9,24]. Meanwhile, note that a couple of wide and vague peaks at about −0.5 V are observed, which can be attributed to the redox reactions of the surface oxygen-containing groups. These functional groups are believed to conduct complex faradic reactions and enhance the pseudocapacitance. But the concentration of electrochemically active functional groups observed by XPS analysis is too low to have a significant impact on the high capacitance of the HHPC.

The Nyquist impedance plot of the carbon-based electrode is shown in Fig. 6b. The inset in the figure shows the expanded high frequency region of impedance. It can be seen that the plot exhibits two distinct traits: a semicircle in the high frequency range and a straight line in the low frequency range. Observing the plot at low frequencies, the points depict shapes close to those of ideal

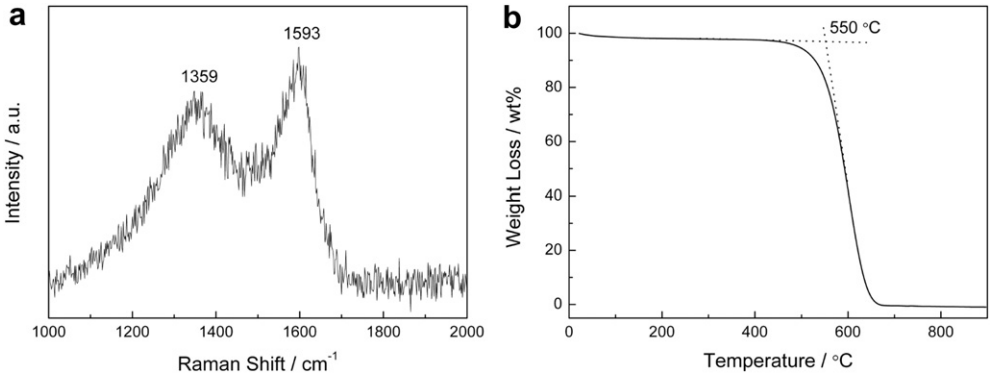

Fig. 3. Raman spectrum (a) and TGA profile (b) of the HHPC.

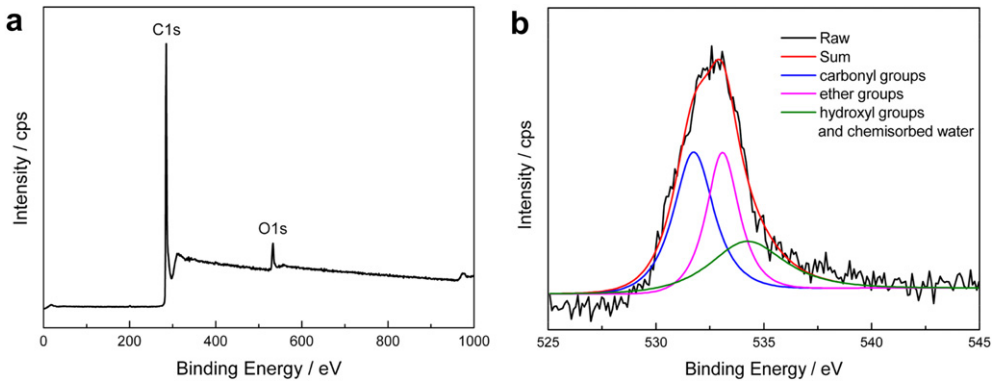

Fig. 4. XPS spectra of the survey scan (a) and O 1s region (b) of the HHPC.

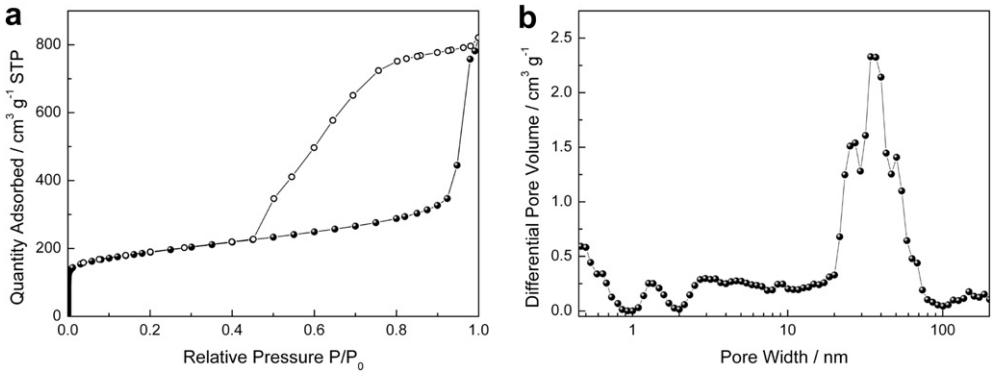

Fig. 5. N_2 adsorption–desorption isotherm (a) and PSD curve (b) of the HHPC.

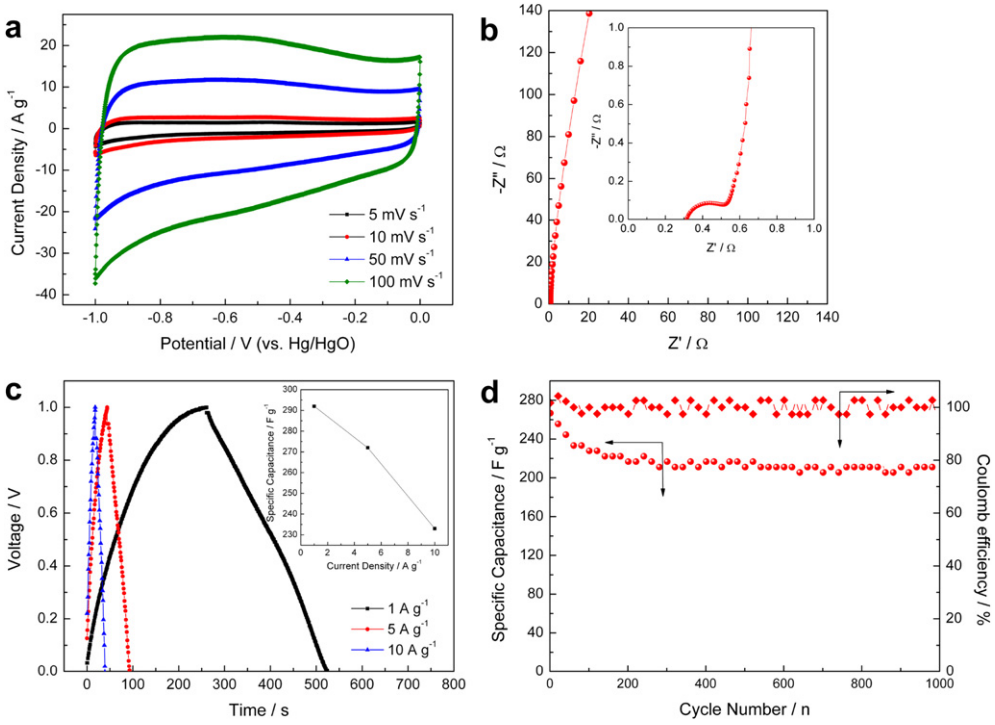

Fig. 6. CV curves at different voltage scan rates (a), Nyquist plot at open circuit potential with amplitude of 5 mV over the frequency range from 100 kHz to 10 mHz (b), plots of potential versus time and variation of specific capacitance (inset) at different current densities (c) and variation of specific capacitance and coulomb efficiency with cycle number at 5 A g^{-1} (d) for the carbon-base electrodes. The inset in (b) shows the expanded high frequency region of impedance.

capacitors. The unconspicuous semicircle at high frequencies associates with the properties of the porous electrode. Generally, the lower the diameter of the semicircle, the higher the mass transfer/diffusion rate of ions through the porous structure of the electrode material. In addition, the value of ESR, including electrolyte resistance, collector/electrode contact resistance and the resistance of the electrode/electrolyte interface, is only 0.30 Ω, which is lower than those reported in previous literature [7,15]. These results demonstrate that the three-dimensional hierarchical porous structure of the HHPC is more helpful for maintaining good capacitive behavior, which can promote the mass transfer/diffusion of ions into the pores effectively.

Galvanostatic charge–discharge measurements were conducted to highlight the capacitance characteristic of the HHPC. Fig. 6c shows the plots of potential versus time and variation of specific capacitance (inset) at different current densities. As shown in the Figure, the charge–discharge curves exhibit almost symmetrical triangle with a slight curvature and have not obvious ohmic drop (iR) related to the internal resistance during the changing of polarity, again showing the small ESR and good capacitive behavior during a rapid charge–discharge process. The specific capacitances of the electrodes are calculated to be 292, 272 and 233 F g^{-1} at 1, 5 and 10 A g^{-1}, respectively. The corresponding capacitances per surface area (C_s) are 44.5, 41.5 and 35.5 μF cm^{-2}, showing high efficient ion-accessible surface area for charge accumulation. The capacitance retention is as high as 80% when the current density increased by 10 times. Obviously, the HHPC exhibits high charge/discharge reversibility and excellent rate capability. This coincides with the CV results and further confirms that the hierarchical porous structure is helpful for ion diffusion and charge accumulation. The variation of specific capacitance with cycle number at 5 A g^{-1} and the corresponding coulomb efficiency are shown in Fig. 6d. During the first 100 cycles, the specific capacitances drop by about 16% from 272 to 228 F g^{-1}, which may be due to the slow reduction of functional groups during cycling in a non-reversible way [25–28]. However, after 100 cycles, the specific capacitance remains almost constant. The coulomb efficiency can reach almost 100% during the whole cycling process, which implies the high reversibility and excellent electrochemical stability of the as-prepared porous carbon.

4. Conclusions

HHPC was prepared through an easy solvent evaporation route using glucose as carbon source and colloidal silica as template. SEM, TEM and N_2 adsorption–desorption results confirm that the HHPC has a three-dimensionally hierarchical pore structure with interconnected meso/macropore and abundant micropore. The electrochemical performances as a supercapacitor electrode material show that the HHPC possesses high specific capacitance (about 292 F g^{-1} at 1 A g^{-1} in KOH aqueous electrolyte), good electrochemical stability and excellent rate capability, which can be mainly attributed to the unique three-dimensional hierarchical porous structure, not only promoting the mass transfer/diffusion of ions into the pores effectively but also offering a good environment for charge accumulation. Therefore, the as-prepared HHPC in this work could be promising as an electrode material for wide application in electrochemical area.

Acknowledgments

This work is financially supported by the National Key Technologies R & D Program of China (2006BAC02A12), National Natural Science Foundation of China (21003077), Natural Science Foundation of Tianjin (08JCZDJC21400) and 111 Project (B12015).

References

[1] L. Wang, T. Morishita, M. Toyoda, M. Inagaki, Electrochim. Acta 53 (2007) 882–886.
[2] A.G. Pandolfo, A.F. Hollenkamp, J. Power Sources 157 (2006) 11–27.
[3] D. Qu, H. Shi, J. Power Sources 74 (1998) 99–107.
[4] F. Li, M. Morris, K.Y. Chan, J. Mater. Chem. 21 (2011) 8880–8886.
[5] B. You, J. Yang, Y.Q. Sun, Q.D. Su, Chem. Commun. 47 (2011) 12364–12366.
[6] H. Yamada, I. Moriguchi, T. Kudo, J. Power Sources 175 (2008) 651–656.
[7] H. Yamada, H. Nakamura, F. Nakahara, I. Moriguchi, T. Kudo, J. Phys. Chem. C 111 (2007) 227–233.
[8] K.S. Xia, Q.M. Gao, J.H. Jiang, J. Hu, Carbon 46 (2008) 1718–1726.
[9] D.W. Wang, F. Li, M. Liu, G.Q. Lu, H.M. Cheng, Angew. Chem. Int. Ed. 47 (2008) 373–376.
[10] J.X. Wang, C.F. Xue, Y.Y. Lv, F. Zhang, B. Tu, D.Y. Zhao, Carbon 49 (2011) 4580–4588.
[11] W.X. Chen, H. Zhang, Y.Q. Huang, W.K. Wang, J. Mater. Chem. 20 (2010) 4773–4775.
[12] Y. Han, X.T. Dong, C. Zhang, S.X. Liu, J. Power Sources 211 (2012) 92–96.
[13] Y. Han, Y.J. Wang, Y.P. Wang, L.F. Jiao, H.T. Yuan, Int. J. Hydrogen Energ. 35 (2010) 8177–8181.
[14] Y. Chen, H. Kim, Fuel Process. Technol. 89 (2008) 966–972.
[15] X.C. Chen, K. Kierzek, Z.W. Jiang, H.M. Chen, T. Tang, M. Wojtoniszak, R.J. Kalenczuk, P.K. Chu, E. Borowiak-Palen, J. Phys. Chem. C 115 (2011) 17717–17724.
[16] R. Demir-Cakan, N. Baccile, M. Antonietti, M.M. Titirici, Chem. Mater. 21 (2009) 484–490.
[17] Z.J. Fan, Q.K. Zhao, T.Y. Li, J. Yan, Y.M. Ren, J. Feng, T. Wei, Carbon 50 (2012) 1699–1712.
[18] Q. Li, R. Jiang, Y. Dou, Z. Wu, T. Huang, D. Feng, J.P. Yang, A.S. Yu, D.Y. Zhao, Carbon 49 (2011) 1248–1257.
[19] T.E. Rufford, D. Hulicova-Jurcakova, K. Khosla, Z.H. Zhu, G.Q. Lu, J. Power Sources 195 (2010) 912–918.
[20] K. Xie, X.T. Qin, X.Z. Wang, Y.N. Wang, H.S. Tao, Q. Wu, L.J. Yang, Z. Hu, Adv. Mater. 24 (2012) 347–352.
[21] W. Li, F. Zhang, Y.Q. Dou, Z.X. Wu, H.J. Liu, X.F. Qian, D. Gu, Y.Y. Xia, B. Tu, D.Y. Zhao, Adv. Energ. Mater. 1 (2011) 382–386.
[22] H.L. Guo, Q.M. Gao, J. Power Sources 186 (2009) 551–556.
[23] J.W. Lang, X.B. Yan, X.Y. Yuan, J. Yang, Q.J. Xue, J. Power Sources 196 (2011) 10472–10478.
[24] F. Xu, R. Cai, Q. Zeng, C. Zou, D. Wu, F. Li, X. Lu, Y. Liang, R. Fu, J. Mater. Chem. 21 (2011) 1970–1976.
[25] E. Frackowiak, F. Béguin, Carbon 39 (2001) 937–950.
[26] V. Khomenko, E. Raymundo-Piñero, F. Béguin, J. Power Sources 195 (2010) 4234–4241.
[27] K. Kierzek, E. Frackowiak, G. Lota, G. Gryglewicz, J. Machnikowski, Electrochim. Acta 49 (2004) 515–523.
[28] C.T. Hsieh, H. Teng, Carbon 40 (2002) 667–674.